3D modelling of β'' in Al–Mg–Si: towards an atomistic level *ab initio* based examination of a full precipitate enclosed in a host lattice

F. J. H. Ehlers[1], S. Dumoulin[2], and R. Holmestad[1]*

[1]Dept. Of Physics, Norwegian University of Science and Technology (NTNU); 7491 Trondheim, Norway

[2]SINTEF, Materials and Chemistry; 7465 Trondheim, Norway

* Corresponding Author: Randi Holmestad

Dept. of Physics, Norwegian University for Science and Technology NTNU, 7491 Trondheim, Norway

email: randi.holmestad@ntnu.no

Tel: +47 7359 3880; Fax: +47 7359 7710

Abstract

We extend a first principles based hierarchical multi-scale model scheme for describing a fully coherent precipitate in a host lattice to 3D simulations. As our test system, the needle-shaped main hardening Al–Mg–Si alloy precipitate β" is chosen. We show that computational costs do not impose practical limits on the modelling: the scheme can probe the full interface energy for physically sized and well isolated precipitates. Examining a series of energetically competitive bulk β" configurations, we highlight a series of results: (i) the scatter in the structural parameters for different β" configurations clearly exceeds experimental uncertainties also when interaction with the host lattice is taken into account. (ii) Structural and compositional β"/Al interfaces generally coincide. This implies that precipitate stoichiometry is retained only for the two β" configurations with the lowest formation energy (compositions $Mg_5Al_2Si_4$, $Mg_4Al_3Si_4$). (iii) β"–$Mg_4Al_3Si_4$ emerges as a minimum energy configuration for large precipitates. Finally, (iv) more complete modelling,

with precipitates surrounded by Al in all three dimensions, is expected to highlight a non-negligible influence of the precipitate misfit along the main growth (needle) direction.

Keywords: First-principles calculations, Aluminium alloys, Precipitate-host lattice interface energies, Multi-scale model scheme

1. Introduction

Age hardenable Al–Mg–Si alloys are widely used due to desirable properties such as high strength-to-weight ratio, good formability and high corrosion resistance. At the heart of understanding the properties of this group of materials are nano-sized precipitates that grow from a supersaturated quenched-in solid solution (SS) upon the 'ageing' heat treatment. These precipitates impede the motion of dislocations in the host lattice, whereby the material acquires its strength. The generally accepted Al–Mg–Si precipitation sequence [1] reads:

$$\text{SS} \rightarrow \text{Mg/Si clusters} \rightarrow \text{GP–zones (pre–}\beta'') \rightarrow \beta'' \rightarrow \text{U1, U2, B', } \beta' \rightarrow \beta, \text{ Si} \quad (1)$$

At peak hardness, the alloy microstructure is dominated by the β" phase [2, 3]. A scenario excluding the influence of other phases well around this point provides an intriguing test-bed for theoretical simulations. The connection between mesoscopic (microstructure) and macroscopic (e.g. materials hardness) system properties in this case can be examined from knowledge of the nucleation, growth and coarsening of a single phase. A well-established modelling framework adopting this strategy exists [4, 5]. That scheme however describes the precipitates in a clearly inaccurate manner, assuming spherical shapes and a constant interfacial energy. By contrast, the experimentally reported β" precipitates [6] are needle-shaped, with non-negligible strain fields and presumed clear interfacial energy differences for at least some of the facets.

For a microstructure model scheme building on the principles outlined above, at least two fundamental motivations behind addressing the influence of more quantitative atomistic level input can be stressed. The authors of [4] used the interfacial energy as a tuning parameter. When this quantity is instead provided by atomistic simulations, along with an appropriately updated precipitate morphology, one would hope to quantify the importance of remaining assumptions in the scheme. In the broader context, the transferability of the model predictions to all relevant material compositions and heat treatments may be significantly improved. Recently [7], the effect of changing the model precipitate morphology from spherical to cylindrical was examined. These studies highlighted a clear influence of an evolving β" aspect ratio on predicted microstructure parameters, motivating further improvements of the relation between β" dimensions and interfacial energy.

The monoclinic β" precipitate (space group C2/m) is characterized [8] by full coherency with the Al host lattice, and planar interfaces in the needle cross-section. Owing to the strong precipitate-host lattice misfits in the cross-section plane, recent arguments in favour of the use of a hybrid model scheme for the interface energy determination in this system have been put forth [9, 10]. It remains to be clarified that the hierarchical multi-scale model scheme proposed in [10] actually improves on presently available alternatives (following the line of thought described in [11]). The motivation of the present studies is not connected with attempts at further increase in precision, however. To our knowledge, there is presently no quantitative information in the literature on the influence of host lattice interactions on the β" structural parameters and formation enthalpies. The aim of this paper is to achieve such information – at a presumed acceptable level of accuracy for preliminary conclusions to be drawn – by extending the scheme of [10] to 3D. Based on the ongoing debate with regards to the β" composition [6, 3, 12], a set of energetically favourable β" configurations (as

opposed to the minimum energy configuration β"–$Mg_5Al_2Si_4$ only) is examined.

The paper is managed as follows: in Section 2, we describe the method framework, with particular focus on the basics of the 3D extension. Model system details for this stage are quantified, and the β" configurations examined are outlined. Section 3 presents the results of the studies, analysing basic features of both the long range, linear elasticity theory (LET) and the short range, density functional theory (DFT) output. Comparison is made with experimental information on the (average) β" cell dimensions and monoclinic angle $\beta_{\beta''}$ in the precipitate cross-section. Section 4 summarizes our work**,** while the basics of the model scheme of [10] are outlined in the appendix. Preliminary work into these issues was presented in [13].

2. Computational details

2.1. Methodology

The basic details of the hierarchical multi-scale model scheme employed in the present work have been described in [10]. Some practical aspects of the modelling are reiterated below (for key equations, see the appendix), with the 3D scheme extensions discussed in Section 2.3. For the LET simulations of the full β"/Al system, finite element modelling (FEM), as implemented in the code LS-DYNA [14] is employed. For simplicity, the subsystem (strain) interactions are characterized here assuming orthotropic elasticity. In a thin (≈ nm width) region enclosing the precipitate-host lattice interface, sequential supercell modelling is performed within the framework of DFT [15, 16]. Here, each individual cell is distorted according to an LET based structural boundary condition. Computational studies [12] suggest that the chosen supercell size (see Section 2.2) is sufficient to incorporate the effects that cannot be described within LET. Strain components along the β" needle directions were neglected in [10], but included in the present work.

On the practical level, the β"/Al system has been modelled following the principles of Eshelby's inclusion approach [17, 18]. At the onset of structural optimization, a compressive displacement field was applied to the precipitate in order to entirely remove subsystem structural parameter differences. The two sets of subsystem nodes located on the interface were merged. The system was then relaxed from this state. All elastic constants used in this full optimization procedure were determined from DFT studies of the isolated subsystems. In the simulations, 256 eight-node elements were employed for each β" slab of unit cell width (for information on the chosen precipitate cross-section dimensions, see Sec. 2.3). For the surrounding Al system, the same density of elements was used only in the region close to β" where the strain field displayed strong variations [10], with the grid being coarser at larger distances. This computation time saving modification had only negligible influence on the strain energy determination.

All DFT calculations have employed Vanderbilt ultrasoft pseudopotentials [19] as implemented in the plane wave based Vienna Ab initio Simulation Package (VASP) [20, 21]. The exchange-correlation functional was approximated using the Perdew-Wang generalized gradient approximation [22] throughout. The chosen PW cut-off in the DFT simulations was 225 eV. A (12, 22, 14) *k*-point grid (1848 irreducible *k*-points) was used for the β" primitive unit cell (see Section 2.2), with appropriate generalizations (a roughly preserved *k*-point density) for the interface cells. Earlier considerations [12] have suggested that this choice of precision is sufficient to provide well converged system energies (interface energy errors within a few percent of a kJ per mole).

2.2. The β" precipitate

The β" structure, as identified by Zandbergen *et al.* [6], is shown in Fig. 1. The experimentally reported [23] β"/Al orientation relationships, also highlighted in this figure, read:

$$[230]_{Al} \parallel [100]_{\beta''}^{Conv.}; [001]_{Al} \parallel [010]_{\beta''}^{Conv.}; [-310]_{Al} \parallel [001]_{\beta''}^{Conv.}. \quad (2)$$

These relationships apply to a β" conventional cell, explaining the superscript 'Conv.' in (2). While the calculations of this work operate with primitive cells (and supercells based on these), the literature typically employs conventional β" cells for structural parameter discussions. We shall follow this general convention here, i.e., the nomenclature {$\mathbf{a}_{\beta''}$, $\mathbf{b}_{\beta''}$, $\mathbf{c}_{\beta''}$} will refer below to the conventional basis vectors of (2). In Fig. 1, the structural differences between these two cells have been outlined. It follows from this information that the first of the relations in (2) should be altered for the β" primitive cell:

$$[231]_{Al} \parallel [100]_{\beta''}^{Prim.}. \quad (3)$$

In the approximation of zero subsystem misfit, the basis vector set {$\mathbf{a}_{\beta''}$, $\mathbf{b}_{\beta''}$, $\mathbf{c}_{\beta''}$} formally transforms into {$\mathbf{a}_H$, $\mathbf{b}_H$, $\mathbf{c}_H$}, where 'H' is an abbreviation for host. Experimentally reported subsystem misfits are discussed below.

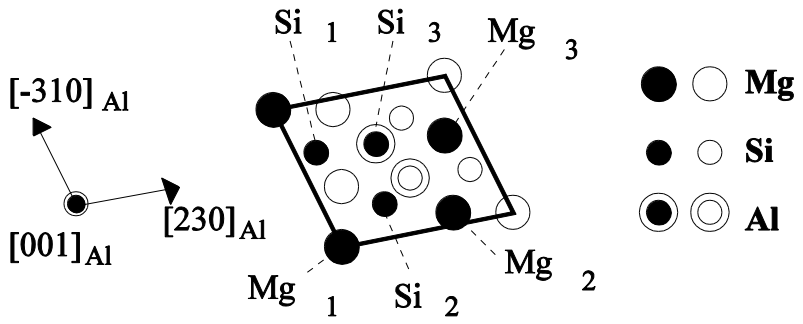

Fig. 1. Schematic illustration of the β" primitive unit cell (selected composition: $Mg_5Al_2Si_4$). The precipitate-host lattice orientation relationships (2) have been highlighted, along with atom types and sites. The conventional β" unit cell is obtained by doubling the cell size along $[230]_{Al}$ ($\mathbf{a}_{\beta''}$).

The β" composition and atom ordering is an ongoing topic of debate. Based on experimentally judged criteria for some of the atom positions, Chen *et al.* [24] computed the relative stability of selected $Mg_{5-x}Al_xSi_6$ configurations, with Si occupying the sites Si_1, Si_2 and Si_3 in Fig. 1. The authors proposed the β"–Mg_5Si_6 configuration as the main candidate, in accordance with earlier transmission electron microscopy (TEM) based work [6, 8]. More recently, atom probe tomography (APT) experiments have strongly suggested the presence of Al on some of these 'Si sites' [3, 25, 26]. Theoretical investigations on larger β" configuration subsets [3] have highlighted β"–$Mg_5Al_2Si_4$ as energetically favoured over β"–Mg_5Si_6, with Al fully occupying the Si_3 sites as shown in Fig. 1. These studies were supported by more recent work [12] where in addition, the possibility of composition fluctuations and disorder, away from sites Si_1, Si_2 and involving Mg and Al only, was stressed. The author of [12] rendered β"–Mg_5Si_6 downright unlikely, as neither bulk precipitate nor interface growth studies provided support for an energetically favourable replacement of Al with Si on the Si_3 sites. All theoretical studies described above used VASP, with the zero temperature formation energies calculated as described in Section 2.4.

For the selection of β" configurations to be examined in the present work, we employed the results of [12], choosing the six energetically most favourable configurations from those studies. Calculated structural parameters and details on the atom ordering for these configurations have been included in Table 1. In practice, our selection procedure implies the following: for each configuration described by a single β" primitive cell, any experimentally proposed constraints on the Mg/Si ratio and phase symmetry are formally ignored. Configuration mixing may still reintroduce these properties for larger precipitate volumes. We still assume, based on results in [3], that the Si_1 and Si_2 sites are occupied exclusively by Si. Finally, we also added β"–Mg_5Si_6 to our investigation, despite the remarks in [12]. This choice was motivated by the ongoing interest in this configuration in the literature, see, e.g., [26–28]. The calculated formation energy of β"–$Mg_5Al_2Si_4$–

I (β"–Mg_5Si_6) in [12] is –0.3456 eV/solute atom (–0.2665 eV/solute atom), with remaining configurations in Table 1 all possessing formation energies below –0.31 eV/solute atom (≈ –30 kJ per mole).

Table 1. Calculated bulk β" structural parameters for the various choices of metastable phase composition and atom ordering selected in this work. The configurations have been ordered according to increasing formation energy, see [12] and Section 3. Unless otherwise noted, the Si (Mg) atoms occupy the sites Si_1, Si_2, Si_3 (Mg_1, Mg_2, Mg_3) in Fig. 1. Experimentally reported parameters have been included at the bottom row. The approximate value for $|\mathbf{b}_{\beta''}|$ here reflects that β" is presumed fully coherent with the Al host lattice along this direction.

Composition (atom ordering)	$\|\mathbf{a}_{\beta''}\|$ (nm)	$\|\mathbf{c}_{\beta''}\|$ (nm)	$\|\mathbf{b}_{\beta''}\|$ (nm)	$\beta_{\beta''}$ (°)
$Mg_5Al_2Si_4$–I (Al: Si_3)	1.532	0.6778	0.4075	105.9
$Mg_4Al_3Si_4$ (Al: Si_3, Mg_1)	1.511	0.6615	0.4131	106.6
Mg_6AlSi_4–I (Al: Si_3; Mg: Si_3)	1.559	0.6830	0.4069	106.1
$Mg_5Al_2Si_4$–II (Al: Si_3, Mg_1; Mg: Si_3)	1.539	0.6692	0.4099	106.5
Mg_6AlSi_4–II (Al: Mg_1; Mg: Si_3)	1.562	0.6734	0.4113	106.2
Mg_7Si_4 (Mg: Si_3)	1.581	0.6898	0.4077	105.4
Mg_5Si_6	1.511	0.6932	0.4080	110.4
(Exp.) [8]	1.516±0.002	0.674±0.002	≈ 0.405	105.3±0.5

Comparison with experimentally reported values (also included in Table 1) suggests a general tendency of both calculated β" cross-section dimensions $|\mathbf{a}_{\beta''}|$, $|\mathbf{c}_{\beta''}|$ to be higher in value. A significant positive precipitate-host lattice misfit has been reported in experiment [8] for both interfaces in the β"/Al cross-section: $m_{\mathbf{a}} = (|\mathbf{a}_{\beta''}| - |\mathbf{a}_H|)/|\mathbf{a}_H| = 3.8\%$; $m_{\mathbf{c}} = 5.3\%$. Considering these observations, the

theoretical discrepancy may be corrected by incorporation of precipitate-host lattice interactions that should have the effect of compressing β". Previous theoretical studies [10] provided direct support for this expectation for β"–$Mg_5Al_2Si_4$–I, but did not quantify the influence on the precipitate cell dimensions. Along the β" needle (main growth) direction $\mathbf{b}_{\beta''}$, the experimental misfit $m_{\mathbf{b}}$ is deemed negligible. By comparison, the calculated values for $m_{\mathbf{b}}$ in Table 1 are always positive, attaining values of up to 2%. For the monoclinic angle $\beta_{\beta''}$, in particular β"–Mg_5Si_6 stands out, with a difference of 5.1° between the calculated and observed value.

2.3. Model system

The model system examined in this work is shown schematically in Fig. 2. Fig. 2a and b describe the full model and physical systems, respectively. Fig. 2c and d highlight details for the model system (individual β"/Al supercells and precipitate cross-section, respectively) for clarity.

Comparing Fig. 2a and b, we stress that the model system has the precipitate enclosed by Al only in the cross-section. This limitation is not due to system size limitations, but a consequence of the present lack of knowledge on the β" needle end interface characteristics. In particular, for this part of the system, experimental information is unavailable, and it is conceivable that the interface is actually incoherent [29]. Primarily for simplicity, we have made the choice here to ignore the issue altogether. For proposed consequences of this assumption, along with considerations on model improvements, see Section 3.

When optimizing the system in Fig. 2a with LET, the slab base (y = 0) is constrained along the needle direction, with all other system dimensions allowed to fully relax. This strategy is not expected to involve practical limitations, however. For the physical system in Fig. 2b, a precipitate symmetry plane along the needle direction would be expected to exist, where the strain components

along the needle direction vanish. The model precipitate in this sense should be viewed as representing only half of the physical one. By contrast, the lack of needle end confinement for the model system in Fig. 2a is presumed to introduce a discrepancy when compared with Fig. 2b. Only close to the bottom of the slab do we hope to describe the physical system with acceptable accuracy.

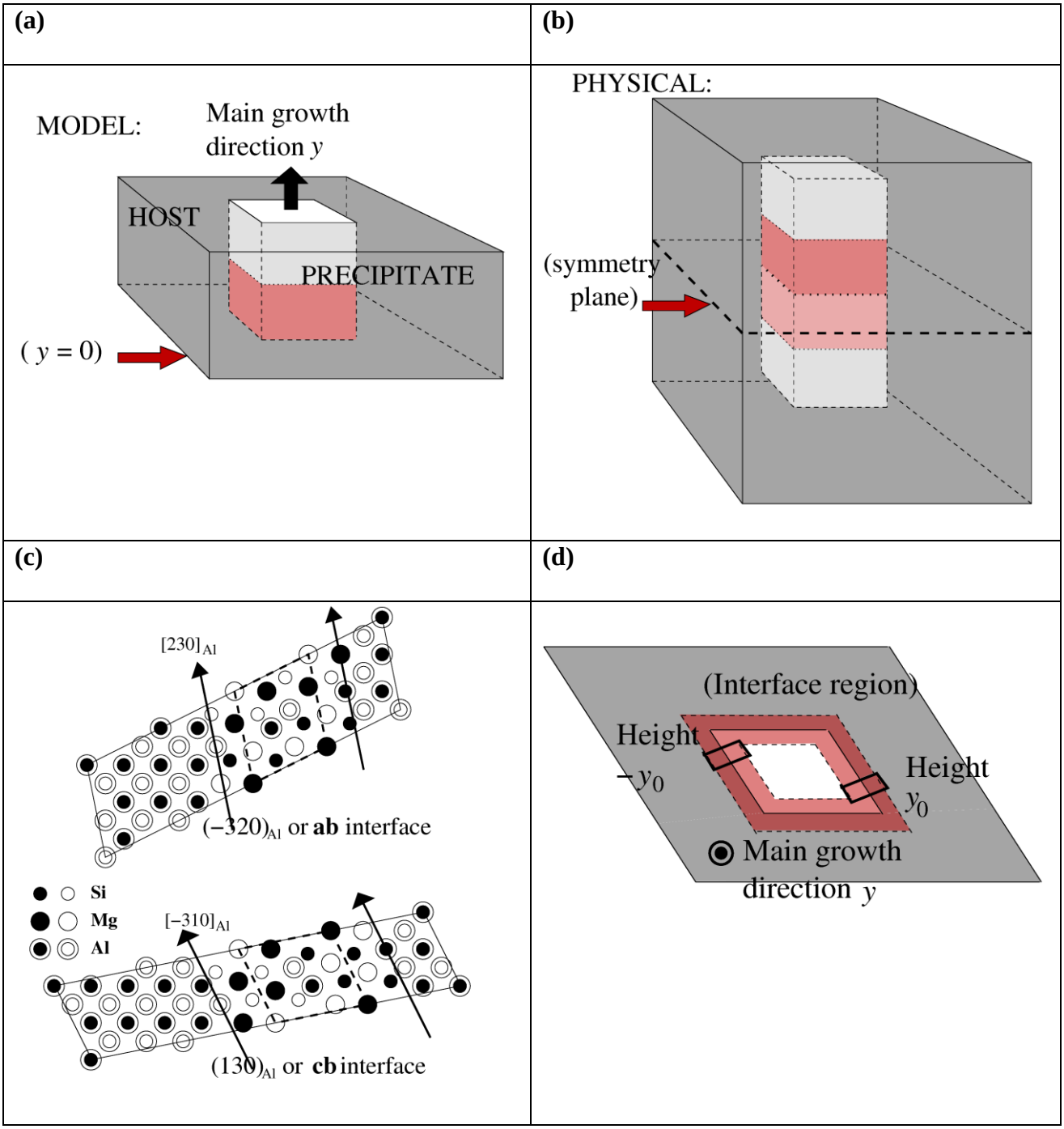

Fig. 2. Schematic illustration of the β"/Al system. (a) The chosen model system geometry subjected to LET studies. Note that the needle-shaped precipitate is only surrounded by host atoms along two

directions. (b) The physical system, with the precipitate fully immersed in the host. Model system comparability is expected only sufficiently far from the needle end (darker precipitate regions in (a), (b)). (c) Atomic structure of the supercells used for the interface region studies. In both figures, a β" primitive unit cell (see Fig. 1) is delimited with broad dashed lines. (d) Schematic presentation of the interface region for a selected height y_0 in the cell. A given supercell couples symmetrically related segments as shown. Thus, the cells in (c) are distorted in general, according to the desired position on the interface.

The above considerations are independent of the detailed features of the (presumed needle-shaped) precipitate under investigation. However, for the actual model scheme implementation, the atomic structures of subsystems and interfaces need to be outlined. Fig. 2c and d provide the necessary information on this issue. In Fig. 2c, the two interface region supercells underlying the DFT studies are drawn. These cells generally (Fig. 2d) comprise symmetrically equivalent pairs of local interface region volumes, with the detailed structural parameters depending on the chosen position on the interface. A β" primitive unit cell (selected configuration $Mg_5Al_2Si_4$–I, see section 2.2) has been highlighted with dashed lines in Fig. 2c.

Both interface region supercells comprise four primitive β" unit cells in terms of number of atoms, divided equally onto the two subsystems. The cell construction follows straightforwardly from the intimate structural connection of precipitate and host lattice. A one-to-one correspondence between the β" and face-centred cubic (fcc) Al sites is present throughout, and only one precipitate atom (located on the Mg_1 site, see Fig. 1) has moved markedly away from its associated host lattice site. As shown in Fig. 2c, the β"/Al interfaces present in the model system are spanned by the β" basis vectors of (2). For this reason, we shall refer to these interfaces as both $\{(-320)_{Al}, (130)_{Al}\}$ and {**ab**, **cb**} throughout this work.

For the model scheme calculations, not only the bulk β" selection, but also the β"/Al interface configurations need to be defined. At the outset, we assumed stoichiometric precipitates throughout, with the interface configurations of Fig. 2c for β"–$Mg_5Al_2Si_4$–I constructed according to this criterion. In order to clarify the interface configuration details for the remaining configurations, we combined the information on atom site modifications and locations from Table 1 and Fig. 1, respectively. For the atoms right at the interface, only the atom type on the Si_3 sites is found to be affected when moving between different bulk β" configurations. For these two Si_3 sites (one per interface), four scenarios are encountered. (i) Both sites occupied by Si (β"–Mg_5Si_6 only). (ii) Both sites occupied by Al (β"–$Mg_5Al_2Si_4$–I and β"–$Mg_4Al_3Si_4$–I). (iii) Both sites occupied by Mg (remaining β" configurations satisfying C2/m symmetry). And finally, (iv) sites occupied by Al and Mg, i.e., different configurations on either side of the supercell precipitate (β" configurations violating C2/m symmetry) [30]. We shall examine the interface configuration selection further in Section 3.4.2.

Based on [10], the following choices were made for the model system cross-section dimensions at the onset of optimization: (i) β": $4|\mathbf{a}_H| \times 8|\mathbf{c}_H|$ (≈ 6 × 5 nm², using $|\mathbf{a}_{Al}| = 0.405$ nm); (ii) fcc Al: 11 times larger along both directions (shape homothetic to the precipitate). This starting point was fixed throughout the work. By contrast, a set of different slab thicknesses – 10, 20, 50, and 100 unit cells along $\mathbf{b}_{\beta''}$ – were examined. Employing the model system symmetry around the slab base, the largest of these thicknesses formally corresponds to a physical precipitate with a length of ≈ 80 nm. Comparing with experimentally reported [2] average β" precipitate dimensions of ≈ 4 × 4 × 50 nm³, realistic precipitate sizes may be well described, depending on the model system accuracy along the β" needle direction. Extending these considerations slightly, we stress that a full 3D scheme, with β" completely surrounded by the host lattice, would be capable of addressing all observed β"

precipitate sizes. The largest model system examined in the present work contains ≈ 1 million 'atoms', largely described as homogeneous media. The number of DFT calculations generally scales with precipitate area (see Section 2.1). Here, each supercell computation (Fig. 2c) is essentially tractable on a desktop.

2.4. Formation and interface energy determination

The calculations performed in the present work compare formation energies at two levels of approximation. Preliminary studies deal with bulk quantities only, i.e., the effects of precipitate-host lattice interactions are ignored. Subsequent considerations add contributions from the interface energies, as determined with the model scheme of [10].

The desired bulk formation enthalpies $\Delta H_{\beta'', \mathrm{Bulk}}$ of a given β"–$Mg_xAl_{7-x-y}Si_{4+y}$ configuration are approximated in the present work with the equations:

$$\Delta H_{\beta'', \mathrm{Bulk}} = H(\beta''\text{–}Mg_xAl_{7-x-y}Si_{4+y}) - x\Delta H_{\mathrm{Mg}}^{\mathrm{SS}} - (7-x-y)\Delta H_{\mathrm{Al}}^{\mathrm{SS}} - (4+y)\Delta H_{\mathrm{Si}}^{\mathrm{SS}}; \quad (4)$$

$$\Delta H_{\mathrm{X}}^{\mathrm{SS}} = H(\mathrm{fcc}\text{–}Al_{107}X) - (107/108)H(\mathrm{fcc}\text{–}Al_{108}). \quad (5)$$

Here, H denotes the enthalpy of the system described in parenthesis. The terms $\Delta H_{\mathrm{X}}^{\mathrm{SS}}$ in (4) approximate the formation enthalpies of the element X in SS, from calculations (5) on a formally isolated atom X in fcc Al. With the quenched-in SS describing the state of the Al–Mg–Si system at the onset of precipitation, negative values of $\Delta H_{\beta'', \mathrm{Bulk}}$ indicate stability of the proposed β" configuration. Throughout the present studies, zero temperature and pressure were assumed. As a consequence of these simplifications, we refer to formation energies ($\Delta E_{\beta'', \mathrm{Bulk}}$) throughout, when discussing our results.

For the computation of the full formation enthalpy for a stoichiometric precipitate, we would generally add two enthalpy contributions to the above predicted $\Delta H_{\beta'', \mathrm{Bulk}}$ values:

$$\Delta H_{\beta'', \mathrm{Full}} = \Delta H_{\beta'', \mathrm{Bulk}} + H_{\mathrm{Int,\ PH}} + H_{\mathrm{Int,\ P+H}}. \quad (6)$$

If the precipitate were fully surrounded by the host, the two new terms would denote subsystem interaction energies for the *full* system. The quantity $H_{\mathrm{Int,\ PH}}$ would include only (DFT) contributions from the interface ('PH') region, shown for a β" cross-section in Fig. 2d, with remaining (LET) interaction energies from both subsystems ('P + H') incorporated in $H_{\mathrm{Int,\ P+H}}$. As discussed in Section 3, the present studies are effectively limited to a 2D slab of unit cell width along the needle direction. For this situation, (6) is modified as

$$\Delta H_{\beta'', \mathrm{Full}} = \Delta H_{\beta'', \mathrm{Bulk}} + H_{\mathrm{Int,\ PH,\ Slab}} + H_{\mathrm{Int,\ P+H,\ Slab}}, \quad (7)$$

with the label 'Slab' highlighting that only part of the full system is probed. For basic details on the computation of the two interface energy quantities, we refer to the appendix. Once again, all practical studies produced formation energies ($\Delta E_{\beta'', \mathrm{Full}}$, etc.). We stress that the quantities in (7) are ultimately determined in units of kJ per mole, with only the solute atoms Mg, Si counted as comprising the various precipitate phases. For a precipitate slab of unit cell height and with cross-section dimensions as described in Section 2.3, the number of atoms in β" thus depends on composition – ranging from 512 (8 × 8 × 8) for the most Al-rich configuration β"–$Mg_4Al_3Si_4$ to 704 (8 × 8 × 11) for the Al-free configurations β"–Mg_5Si_6, β"–Mg_7Si_4.

3. Results and discussion

3.1. Calculated elastic constants

The elastic response of an orthotropic material requires 9 independent parameters, i.e., c_{11}, c_{22}, c_{33}, c_{12}, c_{13}, c_{23}, c_{44}, c_{55} and c_{66}, as opposed to 13 parameters for monoclinic β" [31]. Compared to the β"–$Mg_5Al_2Si_4$–I/Al 2D slab studies of [10], the constants c_{44} and c_{66} attain a practical function when moving into real 3D simulations. In Table 2, all nine calculated elastic constants for the minimum formation energy configuration β"–$Mg_5Al_2Si_4$–I have been included, along with the (three) fcc Al constants. Most of these values were published in previous work by Ehlers and Holmestad [9]. The underlying calculations have employed a coordinate system with **x**, **y** along $\mathbf{a}_{\beta''}$, $\mathbf{b}_{\beta''}$, respectively.

Table 2. Calculated elastic constants for bulk fcc Al and monoclinic β"–$Mg_5Al_2Si_4$–I of Table 1. Experimental values for fcc Al at room temperature (RT) have been added in parentheses for comparison.

Elastic constant	Al (10^{11} N/m²)	β"–$Mg_5Al_2Si_4$–I (10^{11} N/m²)
c_{11}	1.0387[a] (1.0674)[b] (1.068)[c]	1.0897[a]
c_{22}	(= c_{11})	0.8963[a]
c_{33}	(= c_{11})	0.9875[a]
c_{12}	0.6001[a] (0.6041)[b] (0.607)[c]	0.4936[a]
c_{13}	(= c_{12})	0.4308[a]
c_{23}	(= c_{12})	0.5770[a]
c_{44}	0.2936[a] (0.2834)[b] (0.282)[c]	0.2635[d]
c_{55}	(= c_{44})	0.2751[a]
c_{66}	(= c_{44})	0.3234[d]

[a][9] [b][32] [c][31] [d][13]

While our studies involve all β" configurations of Table 1, we decided to simplify our analysis by using the elastic constants for β"–$Mg_5Al_2Si_4$–I throughout for the precipitate part of the system. To ensure that the level of errors in this approximation is secondary to our main conclusions, we examined the sensitivity of the LET strain energies to variations for the presumed most important constants. Four quantities were included in this set: $c_{11} - c_{33}$, dominant in magnitude in general, and c_{55}, describing the shear strain in the precipitate cross-section. In our analysis, we varied these parameters by ±10% around their values in Table 2, focussing on the energy changes at the slab bottom in Fig. 2a. The system was formally divided into four sub parts – β" interior, β" and Al part of the interface region, and host lattice exterior, see Fig. 2d. We found the energy sensitivity to c_{11} and c_{33} from these individual regions to equal or exceed that of c_{55}, with c_{22} being of secondary importance. The latter result is only partly explained by the smaller misfit along $\mathbf{b}_{\beta''}$, and also relates to model system details, discussed in Section 3.2. For c_{11}, the full system strain energy variation over the complete range examined is roughly 1.3% (and closely linear), with by far the largest variations away from the interface region. For c_{55}, interface region energy variations are similar to the c_{11} case, whereas remaining contributions are more than halved. Since an increase in c_{55} raises both subsystem strain energies, the full system sensitivity to this parameter actually slightly exceeds the individual c_{11}, c_{33} variations. More importantly, these numbers strongly suggest that even appreciable variations in the elastic constants have minute influence on the full interface energy for a system structurally closely resembling β"–$Mg_5Al_2Si_4$–I.

For the set of bulk β" configurations in Table 1, β"–Mg_5Si_6 is standing out by its larger monoclinic angle discrepancy on comparison with experiment. A corresponding elastic constant sensitivity analysis for the β"–Mg_5Si_6/Al system (using the calculated full set of bulk β"–Mg_5Si_6 elastic constants, not included in this text) suggested a clearly dominant influence of c_{55}. We view this a

direct consequence of the increased subsystem shear strain due to the poorer coherency for this configuration. Since the calculated value of c_{55} for β"–Mg_5Si_6 is markedly (34%) lower than the β"–$Mg_5Al_2Si_4$–I counterpart, the influence on the strain energy when moving between the two sets of constants is not negligible in this case, but rather reaching 12%. We stress that such a conclusion should apply only to β"–Mg_5Si_6, due to the $\beta_{\beta''}$ discrepancy discussed. Further, since this configuration has the highest formation energy in the set, there is no qualitative influence of the strain energy errors outlined here. In the remainder of this work, unless otherwise noticed, also the β"–Mg_5Si_6/Al system investigations employed β"–$Mg_5Al_2Si_4$–I elastic constants for the precipitate.

Table 3. Selected calculated elastic constants for the full set of β" configurations from Table 1 (where the nomenclature used in the first column is explained).

Configuration	c_{11} (10^{11} N/m²)	c_{22} (10^{11} N/m²)	c_{33} (10^{11} N/m²)
$Mg_5Al_2Si_4$–I	1.0897	0.8963	0.9875
$Mg_4Al_3Si_4$	1.1978	1.0967	1.1496
Mg_6AlSi_4–I	1.1933	1.2135	1.1425
$Mg_5Al_2Si_4$–II	1.0959	1.0682	1.1030
Mg_6AlSi_4–II	1.1485	1.2254	1.1812
Mg_7Si_4	1.0924	1.1291	1.1568
Mg_5Si_6	1.1079	0.9040	0.9799

Finally, we tested the influence of the elastic constants on the precipitate cross-section dimensions and the monoclinic angle. This study was motivated by the observation of strain energy variations within the β" core of close to 20% over the full range of c_{11} changes in the β"–$Mg_5Al_2Si_4$–I analysis. Calculating the values of $c_{11} - c_{33}$ for all β" configurations of Table 1, we performed additional

simulations for each configuration, with these parameters changed compared to the β"–$Mg_5Al_2Si_4$–I set-up. As mentioned previously, this approach would be expected to capture well the behaviour of all configurations but β"–Mg_5Si_6. The computed elastic constants have been included in Table 3. While the scatter in these values is appreciable, the effect on the β" structural parameters was essentially negligible in all cases. This suggests that also the structural considerations of this work (Section 3.3) are reliable, within the model system limitations.

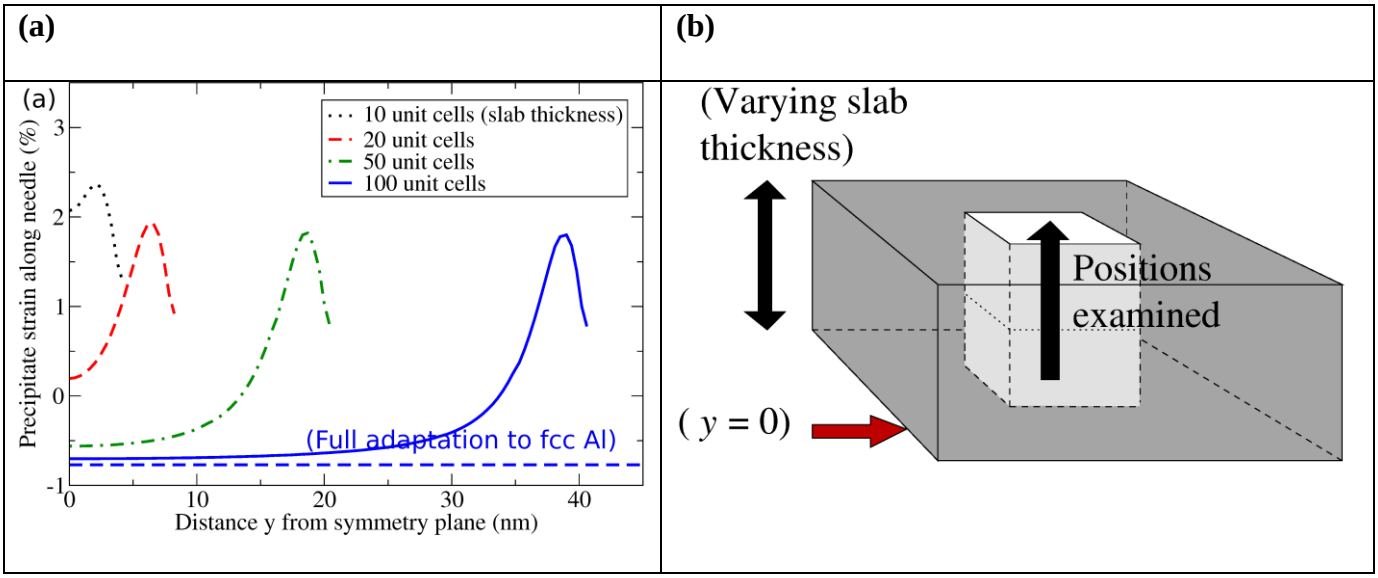

Fig. 3. (a) Calculated precipitate strain along the main growth direction $\mathbf{b}_{\beta''}$ for the β"–$Mg_5Al_2Si_4$–I precipitate with cross-section dimensions $4|\mathbf{a}_{\beta''}| \times 8|\mathbf{c}_{\beta''}|$, as obtained for varying slab thicknesses. (b) Schematic illustration of the analysis. See also Fig. 4.

3.2. System boundary condition

An example of the calculated (LET) precipitate strain along the needle direction $\mathbf{b}_{\beta''}$, as a function of 3D slab thickness (see Section 2.3), has been shown in Fig. 3. These results refer to the lowest formation energy precipitate configuration β"–$Mg_5Al_2Si_4$–I. Studies for the same four thicknesses were also performed for β"–Mg_5Si_6/Al, with the conclusions being essentially equivalent to those described below. For the remaining configurations of Table 1, to be discussed subsequently, only studies for the largest slab were carried out.

Two features are apparent in Fig. 3. Firstly, near the top of the slab, the precipitate is significantly expanded along $\mathbf{b}_{\beta''}$, by ≈ 2% at the peak value. This feature completely dominates the outcome of the precipitate-host lattice interactions for the smallest slab thicknesses. However, as this thickness increases, another behaviour 'emerges' from the slab base. Here, β" is compressed, almost fully adapting to the host lattice along $\mathbf{b}_{\beta''}$ for the largest slab considered. Given that the relative dominance of this latter region is growing with increasing slab thickness, we regard the precipitate expansion as an 'end effect', related to the unphysical nature of the model system.

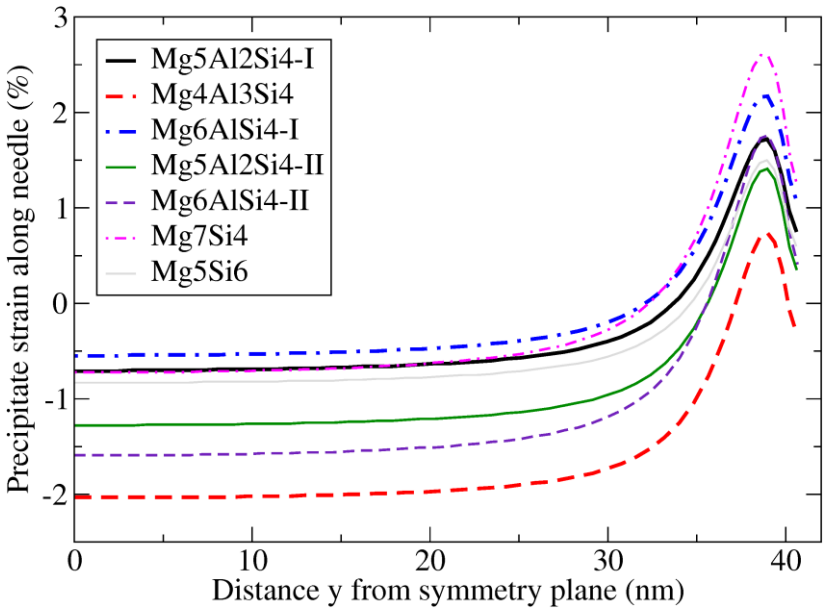

Fig. 4. Calculated precipitate strain along the main growth direction $\mathbf{b}_{\beta''}$ for the full set of β" configurations from Table 1. In all simulations, β"–$Mg_5Al_2Si_4$–I elastic constants, a precipitate with cross-section dimensions $4|\mathbf{a}_{\beta''}| \times 8|\mathbf{c}_{\beta''}|$, and a 100 unit cell thickness were employed.

The results of Fig. 3 on their own provide only limited information on the expected level of confidence in the predicted precipitate behaviour close to the slab bottom. More knowledge on this issue, and the generality of the above conclusions on the larger scale, is obtained from the 100 unit cell slab investigations of the full set of selected β" configurations. As discussed in Section 3.1,

preliminary studies have employed β"–$Mg_5Al_2Si_4$–I elastic constants throughout. The results of these investigations are shown in Fig. 4. The precipitate strain is now strongly varying with the choice of configuration, from roughly –0.5% for one of the β"–Mg_6AlSi_4 configurations to –2.0% for β"–$Mg_4Al_3Si_4$. Comparison of the numerical strain values with the calculated values for the misfit $m_{\mathbf{b}}$ obtained from the bulk configuration data in Table 1 shows a near identity in all cases. In other words, every configuration essentially fully adapts along the needle direction (for heights $y <$ 25 nm) in this analysis. We expect this conclusion to be generalizable to all reasonable choices of β" elastic constants and structural parameters.

Turning to the needle end effects in Fig. 4, we note that the difference between the maximum and minimum strain value over the whole model system is clearly dependent on configuration. Variations in this feature, denoted the 'strain peak height' below, approach 50%. The ordering of these heights does not display a close correlation with the average cross-section misfit values [33] as obtained from Table 1. However, a much better agreement is obtained if comparison is made with an expression where the variable parameter $m_{\mathbf{b}}\gamma$ has been added to $(m_{\mathbf{a}} + m_{\mathbf{c}})/2$, to account for a proposed influence of the misfit along the β" needle direction. Here, the peak height ordering can be almost fully reproduced, for the choice $\gamma \approx 2.2$. This highly qualitative comparison has the purpose of stressing that the strain peak heights may be sensitive to an accumulated subsystem misfit over the *whole* model system. The potential implications of such a conclusion are significant. If a better reproduction of the physical system in Fig. 2b were modelled, the end relaxation effects would almost certainly be distributed more evenly over the system. For such an improved model scheme, we would no longer expect a truly full precipitate adaptation to the host lattice, given the conclusion from Fig. 4 of a non-negligible influence of $m_{\mathbf{b}}$ on the strain peak heights. The simple analysis above does not provide sufficient information to quantify this statement, however. Further, a quantification of this topic is beyond the scope of this paper, given the DFT studies still required to

clarify the configuration(s) for the needle end interface.

3.3. Structural parameters and strain energies

As a consequence of the full β" adaptation to fcc Al along the needle direction for the model system of Fig. 2a (see Section 3.2), we would expect investigations of structural parameters and interface energies to be needed only for a single height in the slab. These suspicions are strongly supported by test calculations, suggesting that variations of the β"–$Mg_5Al_2Si_4$–I interface energies for selected cross-sections (y = 0, 10, and 20 unit cells height) remain within a few percent [34]. Given the strong similarity of the LET results for the different β" configurations, no further tests were performed into this issue. In the remainder of this work, we focus on β" cross-section properties at the height y = 0 only (see Fig. 2a).

Table 4 displays cross-section averaged values for the β" structural parameters $|\mathbf{a}_{\beta''}|$, $|\mathbf{c}_{\beta''}|$ and $\beta_{\beta''}$, for the various configurations examined in Fig. 4. These numbers were obtained from the LET optimized geometries by measuring the lengths of the β" cross-section diagonals and angles at the selected slab height. Compared to the results of Table 1, the scatter in the values of $|\mathbf{a}_{\beta''}|$ and $|\mathbf{c}_{\beta''}|$ for the various configurations examined has been more than halved, but still exceeds experimental uncertainties by close to an order of magnitude. This result indicates that different β" configurations should still be distinguishable in experiment. Comparing the magnitude of the observed and theoretical values in Table 4, we note the opposite trend compared to the discussions in Section 2.2: calculations now predict precipitates *smaller* than experimental findings. As an example, for the lowest formation energy configuration β"–$Mg_5Al_2Si_4$–I, we find that previous discrepancies between theory and experiment of +1.1% (+0.6%) for $|\mathbf{a}_{\beta''}|$ ($|\mathbf{c}_{\beta''}|$) have now been changed into larger differences of –1.3% (–2.2%). The calculated value **of** $\beta_{\beta''}$ remains within experimental error bars. These results first of all imply that the structural effects of incorporating precipitate-host lattice

interactions in the theoretical studies must be rendered non-negligible.

Table 4. Calculated β" structural parameters (cross-section averages), incorporating interactions with the surrounding fcc Al host lattice, for the various β" configurations examined in Fig. 4. These values are practically constant for all heights $y < 25$ nm in the slab. Further, $|\mathbf{b}_{\beta''}| \approx |\mathbf{a}_{Al}|$ for all configurations in this range. Compare with Table 1 for further details.

Precipitate configuration	$\lvert\mathbf{a}_{\beta''}\rvert$ (nm)	$\lvert\mathbf{c}_{\beta''}\rvert$ (nm)	$\beta_{\beta''}$ (°)
$Mg_5Al_2Si_4$–I	1.496	0.6597	105.0
$Mg_4Al_3Si_4$	1.489	0.6532	105.6
Mg_6AlSi_4–I	1.507	0.6629	105.0
$Mg_5Al_2Si_4$–II	1.499	0.6567	105.4
Mg_6AlSi_4–II	1.514	0.6581	105.1
Mg_7Si_4	1.520	0.6658	104.5
Mg_5Si_6	1.486	0.6629	107.5
(Exp.) [8]	1.516±0.002	0.674±0.002	105.3±0.5

We note that all configurations but β"–Mg_7Si_4 and β"–Mg_5Si_6 have the monoclinic angle value within the experimental error bars. Of these two configurations, especially the latter stands out, with the difference of 2.2° being seemingly incompatible with observation [35]. Combined with the strong reservations in [12] with regards to the stability of β"–Mg_5Si_6, admixtures of this configuration in a physical β" precipitate appear unlikely. One should keep in mind at this stage the very limited experimental data presently available [8] for comparison. Evidently, more such data is strongly desired to strengthen the present discussion. From a theoretical perspective, meanwhile, comparison of experimental and structural parameters for phases where both structure and

composition is well established would seem advisable. For this purpose, we have optimized the Al–Mg–Si alloy stable precipitate phase β–Mg_2Si from (1), at a precision matching the choice described in Section 2.1 for the β" studies. Compared to observation for a β phase grown in isolation, our calculated bulk cell dimension of 6.353 Å is ≈ 0.2% above the experimental value [36]. This result may be taken as an indication that any significant bias due to low accuracy in the bulk studies of this work is unlikely.

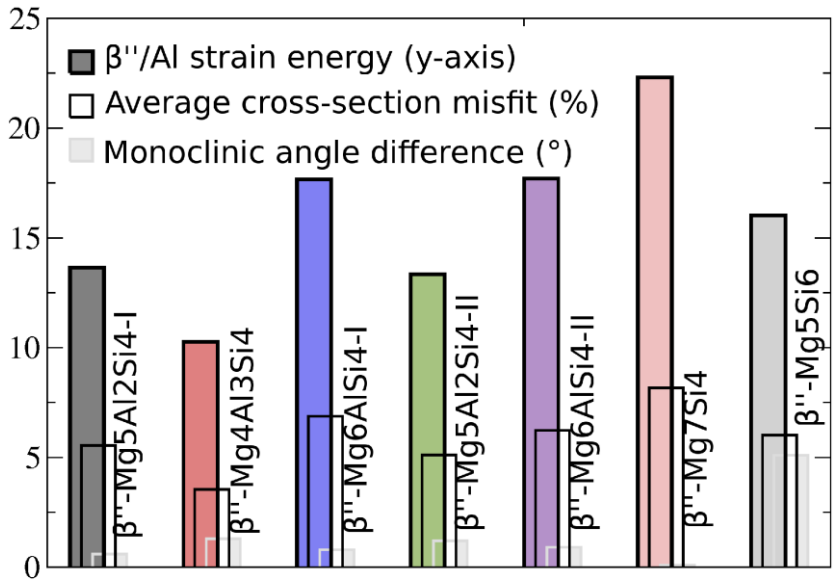

Fig. 5. Comparison of the calculated β"/Al strain energy (in units of kJ per mole × 10^{-1}) with selected bulk β" structural parameters, for the systems of Table 4.

In order to evaluate the relative influence of the various elastic constants on the optimization results of Table 4, we compared the calculated LET strain energies for the y = 0 cross-section with basic bulk β" structural parameters. For attempted clarity, two parameters only were selected; the average misfit in the cross-section $(m_{\mathbf{a}} + m_{\mathbf{c}})/2$ and the numerical difference for the monoclinic angle $\beta_{\beta''}$. The results, ordered according to Table 4, are shown in Fig. 5. A close correlation of the energies with the misfit seems evident for the configurations with $\beta_{\beta''}$ close to the experimental value. For β"–Mg_5Si_6, the analysis is likely prone to significant errors. No strong influence of the large

monoclinic angle discrepancy is revealed in the figure, contrasting the conclusions of Section 3.1. We further note that the values of $m_{\mathbf{a}}$ and $m_{\mathbf{c}}$ differ strongly for this configuration (see Table 1), potentially adding to a different response of this precipitate to the interactions with the host lattice.

Table 5. Calculated β"/Al interface energy contributions for the set of configurations in Table 1. The values $E_{\text{Int, PH, Slab}}$ ($E_{\text{Int, P+H, Slab}}$) are obtained from the interface region of Fig. 2d (remainder of the system), while E_{Int} is the sum of these quantities.

Configuration	$E_{\text{Int, PH, Slab}}$ (kJ/mol at.)	$E_{\text{Int, P+H, Slab}}$ (kJ/mol at.)	E_{Int}, full system (kJ/mol at.)
$Mg_5Al_2Si_4$–I	2.1504	0.8185	2.9689
$Mg_4Al_3Si_4$	1.9702	0.6051	2.5753
Mg_6AlSi_4–I	2.6609	1.0539	3.7148
$Mg_5Al_2Si_4$–II	2.2722	0.7919	3.0641
Mg_6AlSi_4–II	2.4166	1.0523	3.4689
Mg_7Si_4	2.2744	1.3376	3.6120
Mg_5Si_6	1.6843	0.9650	2.6493

3.4. Full interface energies

3.4.1. Stoichiometric precipitates

For the determination of the full interface energies, DFT calculations were required in addition to the LET studies, as described in Section 2.3. The construction of the interface region supercells was discussed in Section 2.1 (see also the appendix), with basic interface configuration details (stoichiometric precipitate assumption) outlined in Section 2.3. The calculated interface energies as obtained from this input have been included in Table 5. Following (7), this output is divided into

two parts: (i) a strain energy $E_{\text{Int, P+H, Slab}}$ from outside the interface region, obtained with LET. (ii) A replacement of the LET energies in the interface region with the quantity $E_{\text{Int, PH, Slab}}$, obtained with DFT.

We find the computed ratio $\{E_{\text{Int, PH, Slab}}\}/\{E_{\text{Int, P+H, Slab}}\}$ to vary with almost 100% for the set of configurations examined, with higher values correlating with more Al-rich β" configurations. In order to qualitatively judge the contributions from electronic interface effects to this variation, we subtracted from the interface region energies the LET strain energies for the same region. For this latter set of numbers, the variation in the corresponding ratio (i.e., the full LET interface region energy divided by $E_{\text{Int, P+H, Slab}}$) is in the range 0.66 – 0.69, i.e., practically unaffected by the choice of β" configuration. The (roughly) estimated interfacial energies obtained from the subtraction still shows a scatter of almost 100%, but with the ordering altered. Now, the highest values are associated with configurations hosting different interface configurations in the supercell (see Section 2.3); β"–Mg_6AlSi_4–I and β"–$Mg_5Al_2Si_4$–II. The lowest values are still connected with the Al-free configurations; β"–Mg_7Si_4 and β"–Mg_5Si_6. We shall discuss the quality of these results further at the end of this section, when examining interface configuration stabilities.

Accompanying the above described variation for the interfacial energies is an almost consistent strain energy increase for increasingly Mg-rich configurations. The latter tendency is explained by the larger precipitate cell volumes induced by these compositional changes (see Fig. 5). From the perspective of precipitate growth, we would generally expect interfacial and strain energies to dominate at early and late stages, respectively. In addition, keeping in mind that β" is believed to grow from its precursor phase pre–β", see, e.g., [37, 25], Table 5 primarily appears to imply a preference for β"–$Mg_4Al_3Si_4$ growth for 'sufficiently large' precipitates, and a preference for an $Mg_5Al_2Si_4$ composition before that point. These qualitative considerations of course may be

strongly influenced by the exact details of the pre–β" phase and the structural transformation to β".

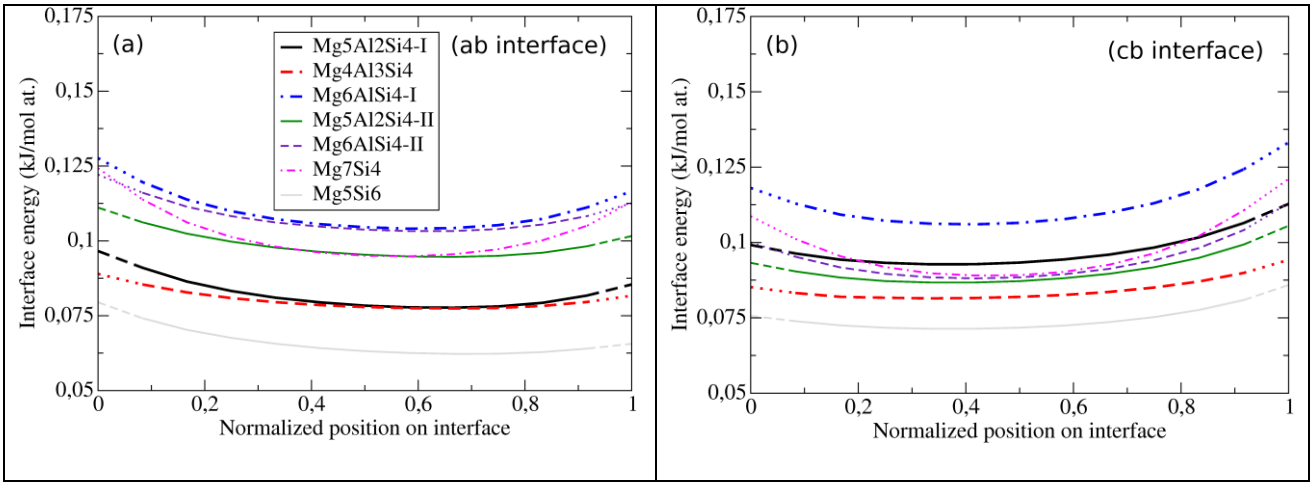

Fig. 6. Contributions to the calculated interface energies from the interface region for the configurations of Table 5. (a) **ab** interface. (b) **cb** interface.

In Fig. 6, the interface energy variation along each interface has been plotted for each configuration. The large variation already evident from Table 5 is clear also here. In addition, however, significant differences are noted for the two interfaces, with, e.g., the β"–Mg_6AlSi_4–II configuration energies for the **cb** interface being comparatively more favourable than the **ab** interface counterpart. Typically, the curvature along the interface for the various curves correlates well with increasing misfit (Fig. 5), with only β"–Mg_5Si_6 displaying a somewhat different trend. Correlations with the misfits also seem evident when comparing the differences in the ordering of the curves in Fig. 6a and b with the structural parameters of Table 1. When moving from the **ab** to the **cb** interface, the misfit for configuration β"–$Mg_5Al_2Si_4$–I increases, while those of configurations β"–$Mg_5Al_2Si_4$–II, β"–Mg_6AlSi_4–II and β"–Mg_7Si_4 decrease. These tendencies are reproduced qualitatively for the interface energies. Once again, β"–Mg_5Si_6 behaves differently. This configuration experiences the largest misfit increase in the above described process, but the **cb** interface energy remains well below that of the other β" configurations. The reason for this different behaviour, already indicated for the full β"/Al system in Fig. 5, remains unexplained at this stage. We still regard it as justifiable

to conclude that the differences between Fig. 6a and b are well explained by misfit variations (as opposed to electronic interactions) for all remaining β" configurations.

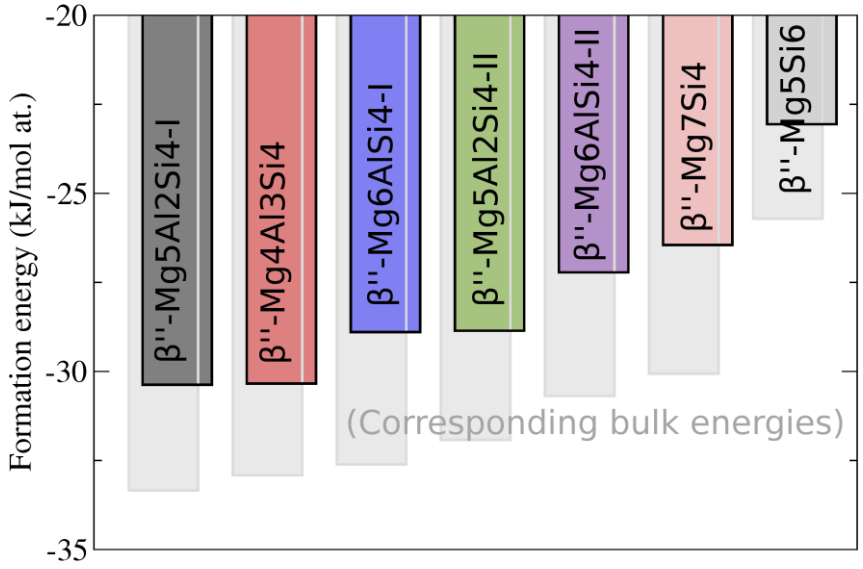

Fig. 7. Calculated β" formation energies, before and after inclusion of the interfacial and strain energy contributions from Table 5.

Fig. 7 shows two sets of energies. (i) The calculated [12] formation energies for the various bulk β" configurations of Table 1. (ii) The updated versions of these quantities when incorporating interactions with the surrounding Al host lattice (Table 5). Although the ordering of the different configurations included in the analysis is unchanged by the strain and interfacial energy contributions, relative stabilizations of certain configurations warrant attention. In particular, the β"–$Mg_5Al_2Si_4$–I precipitate is now only a shared minimum energy configuration, with β"–$Mg_4Al_3Si_4$ possessing essentially the same formation energy. This result should be viewed in the context of the earlier discussion in this section on the growing influence of low strain energies with precipitate size. The model system examined here has dimensions slightly above an average β" precipitate at peak hardness [2]. The results of Fig. 7 indicate that, beyond this point, the β"–$Mg_4Al_3Si_4$ precipitate is favoured. We note that this proposed transition may correlate with the onset of

transition from β" into post–β" phases. Although the formation energies do not provide information on the atomistic β" growth scenario, it is an intriguing thought that a change in the interface growth characteristics may trigger an ultimate structural instability of the β" phase. On the more general level, we stress that the results of Fig. 7 relate to a particular choice of precipitate dimension, and as such cannot be viewed as fully probing the effects of interface energies on the configuration stabilities. In particular, future studies, both experimental and theoretical, should address more closely the most typical cross-section dimensions for the physical precipitates observed.

3.4.2. Beyond stoichiometric precipitates

Up to this point, our computations have assumed stoichiometric precipitates, with consequences to the choice of interface configurations for each bulk β" configuration examined, see Section 2.3. This set-up follows general convention, see, e.g., [29, 9], but nevertheless may be challenged by the well-established dominance of chemical interactions over strain at the interface. Considering the chosen β"–$Mg_5Al_2Si_4$–I interface configurations of Fig. 2c, we note that any bulk β" composition change in Table 1 is affecting this configuration only through second nearest neighbour interactions (atom type substitutions on sites Mg_1, Si_3). Unless we *insist* that the interface configuration should be altered when looking at a different bulk β" configuration, we may well argue that the configuration stability should stay largely unaffected by this modification. This hypothesis seems further strengthened by the discussion in Section 3.4.1. Here, the appreciable variation in the calculated β"/Al interface energies was not explained exclusively by precipitate-host lattice misfit variations, and hence would be expected to relate to the interface configuration differences. Below, we attempt to clarify if a single interface configuration is actually preserved for all β" precipitates considered.

Previous studies into the β"–$Mg_5Al_2Si_4$–I/Al interface configuration stabilities [12] have suggested

that the structural interface (SI) configurations of Fig. 2c are the most stable choices for this bulk β" configuration. Here, the stability was tested against two processes: (i) removal of individual solute atoms from the outermost layer of the precipitate. (ii) Addition of the next layer of solute atoms on a growth path compatible with the chosen bulk β" configuration. Examining fully optimized supercells throughout, any process from the first (second) group was found to always be considerably more (less) favourable compared to the average solute atom binding energy to the precipitate – indicating a long lived SI configuration. For completeness, solute atom additions on the **Si_3 sites** were also considered, with conclusions unchanged. In the present work, we followed the same strategy for the full set of β" configurations of Table 1.

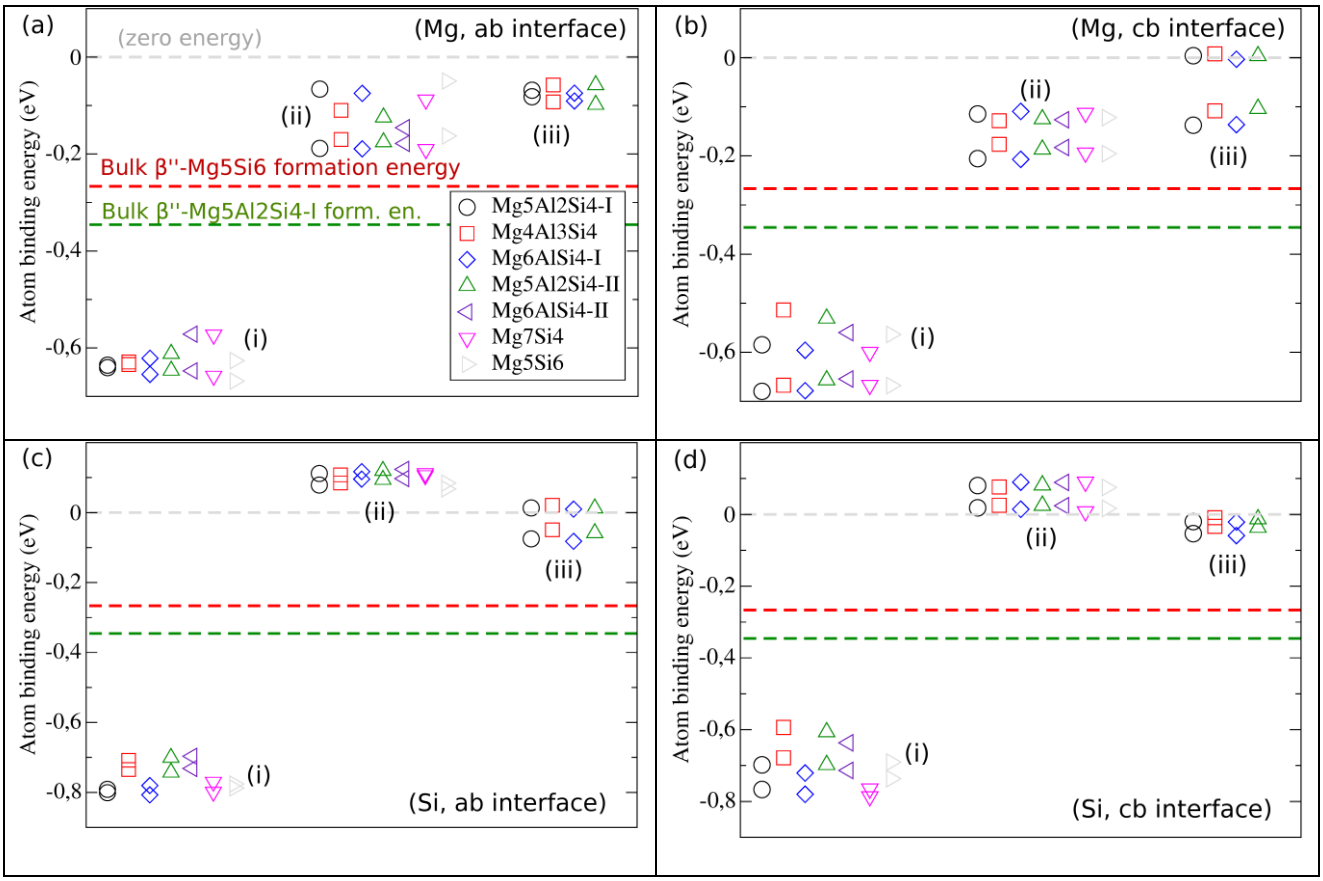

Fig. 8. Calculated single atom binding energies around the structural interface (SI) configuration for the different β" precipitates of Table 1. (a), (b) Mg additions at the **ab** and **cb** interfaces, respectively. (c), (d) Si additions at the **ab** and **cb** interfaces, respectively. In each figure, three clusters of data points are shown: (i) addition of the last atom before completion of the SI

configuration. (ii) Addition of the first atom on a Si_3 site. (iii) Addition of the first atom on a growth path dictated by the bulk β" configuration (for configurations with Al on one or both Si_3 sites in the bulk state).

As shown in Fig. 8, the stability of the SI interface remains supported for essentially all configurations. The outermost solute atom for this configuration is always binding strongly, with an energy of –0.57 eV (–0.51 eV) or lower, for the **ab** (**cb**) interface**.** The next added solute atom, by contrast, is never binding more strongly than –0.19 eV (–0.21 eV). With exception of β"–Mg_5Si_6, this latter value is always well above the bulk β" formation energy, by 0.1 eV or more. Since the Mg_5Si_6 composition has been strongly questioned in both this and previous [12] work, we conclude that the SI configuration stability is well supported in the range of realistic choices of β" compositions. Precipitate stoichiometry, consequently, appears a pure model assumption. According to our studies, some level of Mg enrichment of the SI interface (on the β"–$Mg_5Al_2Si_4$–I Al sites, primarily) is conceivable, whereas Si enrichment appears highly unlikely.

The above result has implications to the calculated interface energy of all precipitates where the stoichiometric interface configuration does not overlap with the SI configuration. This group includes all bulk β" configurations but β"–$Mg_5Al_2Si_4$–I and β"–$Mg_4Al_3Si_4$ – the two lowest energy configurations in Fig. 7. For the two nearest configurations in this figure, β"–Mg_6AlSi_4–I and β"–$Mg_5Al_2Si_4$–II, a rough estimate of the interface energy change upon the interface configuration modification is computed as follows. Removing (in both cases) the outermost Mg atom from the stoichiometric interface, a total of 16 atoms are no longer counted as part of the β" cross-section. With the binding energy of each of these atoms at the interface being ≈ 0.2 eV (figure 8a and b), the bulk phase formation energies being 0.33 – 0.34 eV/atom [12] and the total number of solute atoms in the cross-section being ≈ 700, the interface energy is reduced by ≈ 0.3 kJ per mole. Depending on

the bulk β" configuration, this amounts to almost 10% of the full interface energy in Table 5 – a weak, but non-negligible modification. Upon this correction, the interface energies for the four lowest energy candidates become highly similar. This does not directly indicate stabilization of any new configurations, but it does suggest that precipitate-host lattice interactions have an even weaker effect on relative formation energies than assumed from the results of Section 3.4.1. We also note that the β"–$Mg_5Al_2Si_4$–II configuration may now possess an interfacial energy lower than β"–$Mg_5Al_2Si_4$–I, indicating that compositional disorder in the precipitate could be actively favoured.

3.5. Further improvements in the modelling

The results presented in this work have stressed that modelling the desired system of a precipitate fully surrounded by a host lattice with the scheme of [10] is possible. The present obstacle to performing such studies is formally connected solely with the lack of knowledge (from DFT studies) on the β" needle end interface. The implications of extending the present model system of Fig. 2a to that of Fig. 2b remain to be fully clarified, however. The results of Section 3.2 indicated that the full adaptation of β" to fcc Al along the needle direction may merely be an artefact of the present model system used. If the value of the misfit m_b is influential in deciding the precipitate interface energy and, ultimately, the energetically preferred β" dimensions, this parameter may affect the most likely β" composition non-negligibly. Such a scenario has been discussed for another highly coherent precipitate in recent work by Torsæter *et al.* [38]. Certainly, a build-up of strain along the β" needle direction would be expected to have some influence on the cross-section structural parameters and energies – an issue that has been entirely suppressed in the results of Section 3.3 and 3.4. As such, we can only claim to have highlighted qualitative features in the investigations performed up to now.

Also the limitations to the accuracy in the model scheme itself become apparent when discussing

the structural output in Table 4. As discussed in Section 2.1, the scheme is hierarchical, as opposed to fully self-consistent in its coupling of the DFT and LET simulations. Two main simplifications were identified and discussed already in [10]: firstly, we implicitly assume zero interfacial energy σ for the structural (LET) optimization. If a more realistic value of σ were used, all precipitates would be further compressed. Secondly, the scheme also neglects any influence of DFT subsystem relaxations within the interface region supercells (the β" structural parameters in Table 4 being pure LET results). The effect here for β"–$Mg_5Al_2Si_4$–I is a precipitate expansion [10], counteracting the zero interfacial energy error. These issues should be viewed in the light of the generally small differences between observed and calculated β" structural parameters. Caution is evidently advised at this stage when attempting to quantitatively compare experimental and theoretical information in Table 4 (with the comparatively poorly coherent β"–Mg_5Si_6 being the exception to the rule). For more detailed discussions into potentially fundamental limitations to the accuracy of the scheme, see [10].

We stress that, even with the above issues fully resolved, the model scheme used in this work would have remaining fundamental limitations also in the zero temperature approximation. The scheme assumes defect-free interfaces, hence ignoring dislocations, which are known to provide strain relief for sizeable physical precipitates. Future work is required to increase the model reliability in this context.

4. Summary and conclusion

In this work, we have presented results of a first principles based 3D modelling of the needle-shaped Al–Mg–Si alloy main hardening phase β". Our studies employ an extension of the hierarchical multi-scale 2D scheme described in [10]. For simplicity, and due to our present lack of knowledge on the β" needle end interfaces, our 3D model system involves precipitates enclosed by

fcc Al in two dimensions only. However, examination of isolated β" precipitates – of any desired experimentally observed size – is not prevented by model system size limitations. We have examined a series of β" configurations deemed competitive from bulk formation energy calculations [12]. With precipitate-host lattice interactions taken into account, these configurations are non-negligibly compressed, but still structurally distinguishable. For β"–Mg_5Si_6, the precipitate monoclinic angle $\beta_{\beta"}$ differs from the observed value by ≈ 2°, rendering this configuration unlikely as judged from present experimental knowledge. We find that the same (structural interface) configuration is stabilized for all precipitates, implying that bulk precipitate stoichiometry is preserved only for the two lowest energy configurations β"–$Mg_5Al_2Si_4$–I and β"–$Mg_4Al_3Si_4$. Given the dominant contribution of chemical subsystem interactions to the interface energy, this result implies a weak effect of precipitate-host lattice interactions on relative configuration stabilities. For precipitates somewhat above average size [2], β"–$Mg_4Al_3Si_4$ does appear to be stabilized relative to β"–$Mg_5Al_2Si_4$–I. It is however unclear whether this transition is taking place when the β" precipitate itself has started transforming into post-β" phases. Finally, we observe indications that the misfit along the β" needle direction may have additional influence on relative configuration formation energies. This may trigger compositional disorder, as discussed previously in [38].

Acknowledgements

This work has been financially supported by the Research Council of Norway via the MultiModAl project (Project No. 205353). DFT simulations were performed through access to the NOTUR facilities.

Appendix

The present appendix discusses the basic equations used for constructing the distorted interface region supercells of the β”/Al interface region in figure 2d, while also clarifying the

energy contributions to (7).

As discussed in section 2.1, the modelling proceeds from an LET optimization of the full β”/Al system, with only the narrow interface region enclosing the precipitate-host lattice interface ultimately subjected to DFT studies. As indicated in figure 2d, this region is comprised in practical studies by a "patchwork" of β”/Al supercells (examples shown in figure 2c). Each cell is subjected to distortions specific to the chosen position on the interface, as obtained directly from the LET output of the full system simulations. Given the periodic boundary constraints on the supercells, the task at hand is a determination of the cell dimensions $\{a^{ab}(i), b^{ab}(i), c^{ab}(i)\}$ for each **ab** interface cell *i*, and likewise $\{a^{cb}(j), b^{cb}(j), c^{cb}(j)\}$ for each **cb** interface cell *j*. Here *i, j* are parameters specifying the position on the interface.

It was shown in [10] that we may write, for the basis vectors along each interface in the precipitate cross-section,

$$a^{ab}(i) = |(a_{H,\,LET}(i) + a_{\beta”,\,LET}(i))/2| * a_H/|a_H|, \qquad \text{(A1)}$$

$$c^{cb}(j) = |(c_{H,\,LET}(j) + c_{\beta”,\,LET}(i))/2| * c_H/|c_H|, \qquad \text{(A2)}$$

where the subscript 'LET' emphasizes that values are to be obtained from the FEM simulations. By contrast, the cell dimensions out of the interface in the precipitate cross-section were not specified by a rigorous equation. Rather, these values were argued to be deducible from the distance of nodes on either side (precipitate, host lattice) of the interface region - selected according to the chosen value of *i* (*j*), and separated by $|a_H|$ ($2|c_H|$) at the onset of system optimization.

For the cell dimension out of the interface, the considerations of [10] do not apply, as strain

components along this direction are now taken into account. As discussed in section 3.3, investigations in the present work concentrate on the region where β” fully adapts to Al along the precipitate needle direction. Consequently, for all *i*, *j*,

$$b^{ab}(i) = b^{cb}(j) = b_H. \qquad \text{(A3)}$$

The last two terms in (7), together comprising the interface energy of the selected β”/Al slab with unit cell width along the precipitate needle direction, can now be obtained as outlined previously in [10]. For the contributions outside of the interface region, computed within LET,

$$E_{\text{Int, P+H, Slab}} = \zeta_{\beta''} N_{\beta''} + \zeta_H N_H, \qquad \text{(A4)}$$

where $\zeta_{\beta''}$, e.g., denotes the strain energy in the precipitate interior, with $N_{\beta''}$ being the number of atoms contained in this region. For the interface region contributions, calculated within DFT,

$$\begin{aligned} E_{\text{Int, PH, Slab}} \quad &= \Sigma_i \{E_{PH}(a^{ab}(i), b^{ab}(i), c^{ab}(i)) - (N_{\beta'',ab}/N^{ab})E_{\beta''} - (N_H{}^{ab}/N^{ab})E_H\} \\ &+ \Sigma_j \{E_{PH}(a^{cb}(j), b^{cb}(j), c^{cb}(j)) - (N_{\beta'',cb}/N^{cb})E_{\beta''} - (N_H{}^{cb}/N^{cb})E_H\}. \qquad \text{(A5)} \end{aligned}$$

Here, the energies in the first set of brackets denote, respectively, the full energy of **ab** interface region supercell *i*, the energy of a bulk β” conventional unit cell and the energy of a bulk fcc Al supercell with basis vectors $\{a_H, b_H, c_H\}$ (see section 2.2). The latter two energies have been suitably scaled to ensure that bulk phase contributions to the energy are eliminated; $N_{\beta'',ab}$ ($N_H{}^{ab}$) denotes the number of atoms in the two bulk cells, while the number of atoms in the β”/Al supercell is given as $N^{ab} = N_{\beta'',ab} + N_H{}^{ab}$. Corresponding considerations apply to the **cb** interface contributions to $E_{\text{Int, PH, Slab}}$. The parameters *i*, *j* are summed over the full interface included in the slab.

References

[1] G. Edwards, K. Stiller, G. Dunlop, and M. Couper, Acta Mater. **46**, 3893 (1998).

[2] C.D. Marioara, S. J. Andersen, H. W. Zandbergen and R. Holmestad, Metal. Mater. Trans. A **36A** 691 (2005).

[3] H. S. Hasting, A. G. Frøseth, S. J. Andersen, R. Vissers, J. C. Walmsley, C. D. Marioara, F. Danoix, W. Lefebvre, and R. Holmestad, J. Appl. Phys. **106**, 123527 (2009).

[4] O. R. Myhr and Ø. Grong, Acta Mater. **48**, 1605 (2000).

[5] O. R. Myhr, Ø. Grong, H. G. Fjær, and C. D. Marioara, Acta Mater. **52**, 4997 (2004).

[6] H. W. Zandbergen, S. J. Andersen and J. Jansen, Science **277**, 1221 (1997).

[7] A. Bahrami, A. Miroux, and J. Sietsma, Metal. Mater. Trans. A **43A**, 4445 (2012).

[8] S. J. Andersen, H. W. Zandbergen, J. Jansen, C. Træholt, U. Tundal, and O. Reiso, Acta Mater. **46**, 3283 (1998).

[9] F. J. H. Ehlers and R. Holmestad, Comput. Mater. Sci. **72**, 146 (2013).

[10] F. J. H. Ehlers, S. Dumoulin, K. Marthinsen, and R. Holmestad, Model. Simul. Mater. Sci. Eng. **21**, 085018 (2913).

[11] V. Vaithyanathan, C. Wolverton and L. Q. Chen, Acta Mater. **52**, 2973 (2004).

[12] F. J. H. Ehlers, Comput. Mater. Sci. **81**, 617 (2014).

[13] F. J. H. Ehlers, S. Dumoulin, and R. Holmestad, Proceedings of the 2nd World Congress on Integrated Computational Materials Engineering (ICME), Ed. M. Li, C. Campbell, K. Thornton, E. Holm, and P. Gumbsch, TMS, Wiley (2013), ISBN 978-1-11876-689-7, p. 189.

[14] J.O. Hallquist, LS-DYNA Keyword User's Manual Version 971, California: Livermore Software Technology Corporation (2007).

[15] P. Hohenberg and W. Kohn, Phys. Rev. **136**, B864 (1964).

[16] W. Kohn and L. J. Sham, Phys. Rev. **140**, A1133 (1965).

[17] J. D. Eshelby, Proc. Roy. Soc. A **24**, 376 (1957).

[18] C. Q. Ru, Acta Mech. **160**, 219 (2003).

[19] D. Vanderbilt, Phys. Rev. B **32**, 8412 (1985).

[20] G. Kresse and J. Hafner, Phys. Rev. B **47**, R558 (1993).

[21] G. Kresse and J. Furthmüller, Comput. Mater. Sci. **6**, 15 (1996).

[22] J. P. Perdew, J. A. Chevary, S. H. Vosko, K. A. Jackson, M. R. Pederson, D. J. Singh, and C. Fiolhais, Phys. Rev. B **46**, 6671 (1992).

[23] G. A. Edwards, K. Stiller, G. L. Dunlop, Appl. Surf. Sci. **76/77**, 219 (1994).

[24] J. H. Chen, E. Costan, M. A. van Huis, Q. Xu, and H. W. Zandbergen, Science **312**, 416 (2006).

[25] G. Sha, H. Möller, W. E. Stumpf, J. H. Xia, G. Govender, and S. P. Ringer, Acta Mater. **60**, 692 (2011).

[26] S. Pogatscher, H. Antrekowitsch, H. Leitner, A. S. Sologubenko, and P. J. Uggowitzer, Scripta Mater. **68**, 158 (2013).

[27] H. Zhang, Y. Wang, S. L. Shang, C. Ravi, C. Wolverton, L. Q. Chen, and Z. K. Liu, Calphad **34**, 20 (2010).

[28] R. Yu, J. Zhu, and H.Q. Ye, Comp. Phys. Commun. **181**, 671 (2010).

[29] Y. Wang, Z.-K. Liu, L.-Q. Chen and C. Wolverton, Acta Mater. **55**, 5934 (2007).

[30]: For the last set of configurations, a different supercell is created when performing a permutation of the two interface atoms highlighted in the discussion. The effect of such permutations was checked throughout, and found to change the interface energy by no more than 0.05 kJ per mole (i.e., a few percent).

[31] C. Kittel, Introduction to Solid State Physics, 8th Ed., Wiley (2005), ISBN: 0-471-41526-X, p. 77.

[32] J. F. Thomas, Phys. Rev. **175**, 955 (1968).

[33] The misfits $m_{\mathbf{a}}$ and $m_{\mathbf{c}}$ are averaged here to reflect the similar length of the precipitate sides in the model system cross-section; $4|\mathbf{a}_{\beta''}| \approx 8|\mathbf{c}_{\beta''}|$.

[34] For the DFT part of the underlying studies here, we employ an additional symmetry for the optimized model system geometry: the two halves of the interface region supercell in Fig. 2d can be chosen for the same height without loss of generality, i.e., the transformation $-y_0 \rightarrow y_0$ is allowed.

[35] When β"–Mg_5Si_6 elastic constants are used for the simulation (see Section 3.1), this difference is reduced to 1.6° – still more than three standard deviations from the experimental value.

[36] O. Madelung, Landolt-Börnstein Numerical Data and Functional Relationships in Science and Technology, New Series, Group III, Springer-Verlag: Berlin (1983), Vol. 17e, pp. 163, 432.

[37] C. D. Marioara, S. J. Andersen, J. Jansen, and H. W. Zandbergen, Acta Mater. **49**, 321 (2001).

[38] M. Torsæter, F. J. H. Ehlers, C. D. Marioara, S. J. Andersen, and R. Holmestad, Philos. Mag. **92**, 3833 (2012).